Dalton Transactions

ROYAL SOCIETY OF CHEMISTRY

PAPER

View Article Online
View Journal | View Issue

Cite this: *Dalton Trans.*, 2023, **52**, 6870

Persilylation of ferrocene: the ultimate discipline in sterically overcrowded metal complexes†

Susanne M. Rupf, [a] Robin Sievers,[a] Paulin S. Riemann,[a] Marc Reimann, [b] Martin Kaupp, [b] Carlo Fasting[a] and Moritz Malischewski *[a]

Received 14th April 2023,
Accepted 19th April 2023

DOI: 10.1039/d3dt01133j

rsc.li/dalton

We report the preparation and structural characterization of the first persilylated metallocene *via* the metalation of decabromoferrocene. Although Grignard conditions turned out to be insufficient due to the steric and electronic effects of silyl groups causing a decreased nucleophilicity of the metalated intermediates, stepwise lithium–halogen exchange yields complex mixtures of polysilylated compounds $FeC_{10}DMS_nH_{10-n}$ (n = 10, 9, 8) including the targeted decasilylated ferrocene. These mixtures were successfully separated allowing a systematic study of silylation effects on ferrocene by XRD, CV, NMR and UV/vis spectroscopy supported by DFT calculations. The findings were used to develop a high-yielding and simple preparation method to generate a tenfold substituted overcrowded ferrocene, $FeC_{10}DMS_8Me_2$.

Introduction

Given the outstanding variety of possible cyclopentadienyl (Cp) complexes reported so far, cyclopentadienyl ligands with dimethylsilyl (DMS) or trimethylsilyl (TMS) groups have found widespread synthetic applications. As they are superior in steric demand to the corresponding carbon containing analogues, iso-propyl and *tert*-butyl,[1,2] they allow the isolation of reactive f-block[3–7] and main group complexes[8–12] and improve hydrocarbon solubility.[13] Moreover, the introduction of silyl groups allows the generation of sensitive (redox) species due to hyperconjugation effects, allowing the isolation of highly reduced organic compounds[14–18] or low-valent actinide and lanthanide compounds, like $\{[C_5H_{5-n}(SiMe_3)_n]_3M\}^{1-}$ (n = 1, 2), containing metal centers with a formal oxidation state of +II as demonstrated by the Evans group.[19–24] Although higher degrees of silylation are expected to result in an increased kinetic stability of low-valent species due to steric demand and changed electronic properties of the Cp ligand, the steric overload required and the further changed electronic properties of the Cp ligands pose a formidable synthetic challenge.

So far, only one transition metal complex with a pentakis (dimethylsilyl) substituted Cp ligand is known in the literature. Sünkel and Hofmann prepared $[Mn(CO)_3(C_5DMS_5)]$ by iterative lithiation and silylation of $[Mn(CO)_3(C_5Br_5)]$ (Scheme 1, top).[25]

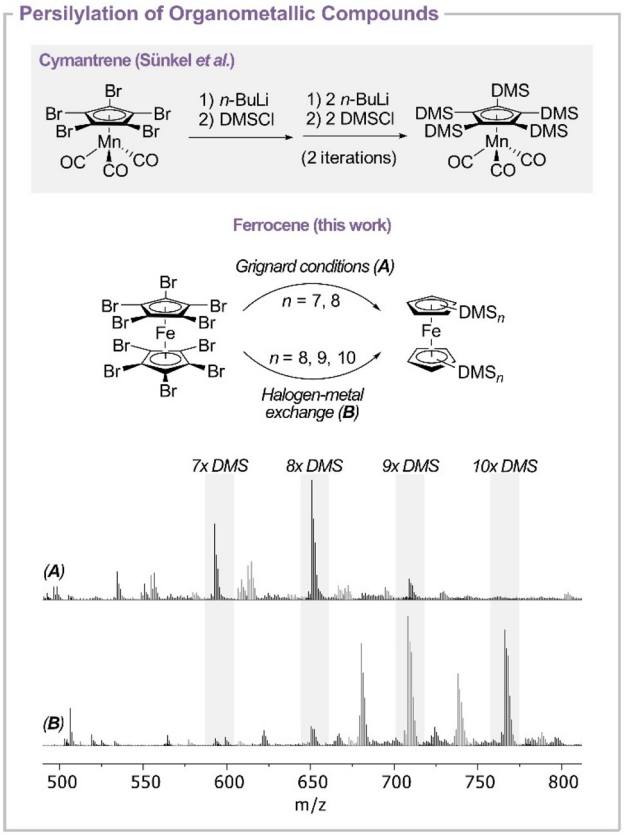

Scheme 1 Overview of synthetically prepared persilylated compounds. Top: persilylation of $[Mn(CO)_3(C_5Br_5)]$ by iterative lithium–halide exchange and reaction with DMSCl. Middle: silylation of $[FeC_{10}Br_{10}]$ with DMSCl *via* lithium–halogen exchange and Grignard reaction. Bottom: the corresponding mass spectra of the conversions.

[a]*Freie Universität Berlin, Fabeckstr. 34-36, 14195 Berlin, Germany. E-mail: moritz.malschewski@fu-berlin.de*
[b]*Technische Universität Berlin, Straße des 17. Juni 135, 10623 Berlin, Germany*

†Electronic supplementary information (ESI) available. CCDC 2248053 (**1**), 2248054 (**2**), 2248060 (**3a**), 2248059 (**3b**), 2248057 (**4a**), 2248058 (**4b**), 2248056 (**5**) and 2248055 (**6**). For ESI and crystallographic data in CIF or other electronic format see DOI: https://doi.org/10.1039/d3dt01133j

Although the preparation of $[C_5DMS_5]^-$ by the reaction of C_5DMS_6 with MeLi has been reported,[26] it has never been used for follow-up chemistry. Here, the corresponding C_5DMS_6 was prepared by the reaction of C_5Br_6 with Mg and DMSCl. Claims in the Russian literature regarding the preparation of C_5TMS_6 [27] were not reproducible. In contrast, the synthesis of $[C_5TMS_3H_2]^-$ is well established and the ligand is easily coordinated in reactions with metal halides.[28–31] However, the synthetic challenge becomes more demanding for metallocenes due to the repulsion of the sterically crowded Cp ligands in the "sandwich" structure. Okuda achieved high silylation degrees by the reaction of iron(II) halides with tris(1,2,4-TMS) cyclopentadienyllithium to yield 1,1′,2,2′,4,4′-hexakis(trimethylsilyl)ferrocene. As a consequence of the steric demand, a distorted structure of the silylated Cp ligands is observed.[32] Butler *et al.* reported an alternative approach for hexakis(trimethylsilyl)ferrocene including a lithium–halogen exchange of 1,1′,2,2′,3,3′-hexabromoferrocene followed by silylation with TMSCl.[33] Recently, some of us reported an improved synthetic protocol for decabromoferrocene[34] by the bromination of $[FeC_{10}(Hg(O_2CC_3H_7)_{10}]$.[35] The reaction pathway emerging from perbrominated ferrocene is supposed to be a promising route to persilylation. In the context of ferrocene as a highly versatile model compound in organometallic chemistry,[36] we were interested in synthesizing the first persilylated ferrocene to investigate the resulting steric and electronic effects.

Results and discussion

Unsubstituted ferrocene

One major challenge in converting $[FeC_{10}Br_{10}]$ effectively into the subsequent silylated ferrocene was to avoid trapping of protons by basic intermediates. Therefore, the reaction itself and especially the used solvents and silanes as well as the glassware had to be made as dry as possible (ESI, S1†). The persilylation of $[FeC_{10}Br_{10}]$ was carried out by a direct reaction with elemental magnesium or by bromine–lithium exchange followed by subsequent trapping with a suitable DMS electrophile (Scheme 1, bottom). Herein, the degree of silylation was followed by mass spectrometry.

All reactions including Grignard formation were carried out using DMSCl or DMSOTf in tetrahydrofuran (THF) by varying the conditions like temperature and reaction time (ESI, Table S1†). For all reactions, mass spectrometry revealed that the Grignard formation was complete as no brominated species were observed. However, the silylation step seems to proceed very slowly at high degrees of silylation, as the formation of decasilylferrocene (m/z = 766.2530 for $[FeC_{10}DMS_{10}]^+$) was only observed in traces. Instead, mixtures of $[FeC_{10}DMS_7H_3]$ (m/z = 592.1711 for $[FeC_{10}DMS_7H_3]^+$) and $[FeC_{10}DMS_8H_2]$ (m/z = 650.1946 for $[FeC_{10}DMS_8H_2]^+$) as main products were obtained (Scheme 1, bottom) in the presence of DMSCl indicating that the nucleophilicity of the Grignard species $\{FeC_{10}DMS_n(MgBr)_{10-n}\}$ (n = 8, 9, 10) is decreased with every DMS group attached to it. Therefore, additional reactions were carried out with DMSOTf as a more electrophilic silylation reagent. In the reactions including DMSOTf, however, silylation of the attached DMS groups takes place rather than the formation of persilylferrocene, causing oligomerization of the attached silyl groups as well as polymerization of the solvent.

As the generated silylated Grignard intermediates seem to be too unreactive for further silylation, to give the target $[FeC_{10}DMS_{10}]$, organolithium compounds were used instead. Herein, lithium is introduced by lithium–halogen exchange with ^{t}BuLi and $FeC_{10}Br_{10}$ followed by the addition of DMSCl. The introduction of lithium in the *ortho*-position to bromine can cause a subsequent elimination of lithium bromide, which is known for several aryls followed by aryne formation and decomposition.[37,38] Therefore, a lithiation agent and an electrophile were added at −100 °C. The stability of the lithiated species varies depending on the solvents. While in *n*-pentane the compounds only decompose slowly at room temperature, which can be explained by the low solubility in alkanes, in THF and Et_2O decomposition was observed above *ca.* −80 °C. The silylation itself was mainly observed between *ca.* −80 °C and room temperature in THF and in *n*-pentane between −50 °C to room temperature indicating that the silylation proceeds faster in THF. However, in Et_2O the lithiated intermediates decompose before the silylation process starts. The mass spectra of the reactions in THF and *n*-pentane still revealed incomplete substitution as after the first lithiation attempt with up to 80 equivalents of ^{t}BuLi, in both cases brominated species were still visible at m/z = 672.0876 for $[FeC_{10}DMS_7BrH_2]^+$, m/z = 730.1196 for $[FeC_{10}DMS_8BrH]^+$, m/z = 750.0010 for $[FeC_{10}DMS_7Br_2H]^+$, m/z = 788.1330 for $[FeC_{10}DMS_9Br]^+$ and m/z = 808.0328 for $[FeC_{10}DMS_8Br_2]^+$ (ESI, Fig. S57†). Here, the compounds $[FeC_{10}DMS_8Br_2]$ (**1**) and $[FeC_{10}DMS_9Br]$ (**2**) were isolated and characterized (see the ESI†). Due to the presence of brominated species in the mass spectra, we exclude the formation of $[FeC_{10}Li_{10}]$ as the main intermediate of the reaction. Improved conversion is achieved by multiple metalation cycles. Here, the choice of the solvent becomes more important after multiple lithiation and silylation iterations. While after four iterations in *n*-pentane brominated species are still visible in the mass spectra, in THF three iterations are sufficient to transform all brominated compounds. However, the formation of side products at m/z = 606.1510 ($FeC_{25}H_{54}Si_7$), m/z = 680.2075 ($FeC_{28}H_{64}Si_8$) and m/z_{found} = 738.2315 ($FeC_{30}H_{70}Si_9$) is observed (Fig. 1, bottom). As *n*-pentane still offers sufficient reaction speed it was chosen to be the most suitable solvent for the first lithiation and later changed to THF to reduce side reactions. Nevertheless, *via* this approach we were able to isolate the desired $[FeC_{10}(DMS)_{10}]$ (**6**) in milligram amounts.

The persilylated derivative is only poorly soluble in most organic solvents but can consequently be easily separated by crystallization from THF or *n*-pentane to afford compound **6** as a purple solid. Further purification of the remaining polysilylated metallocene mixtures was accomplished by reverse phase HPLC, using methanol/water as the eluent. Starting from the crude mixture not only were the hepta-, octa-, nona- and

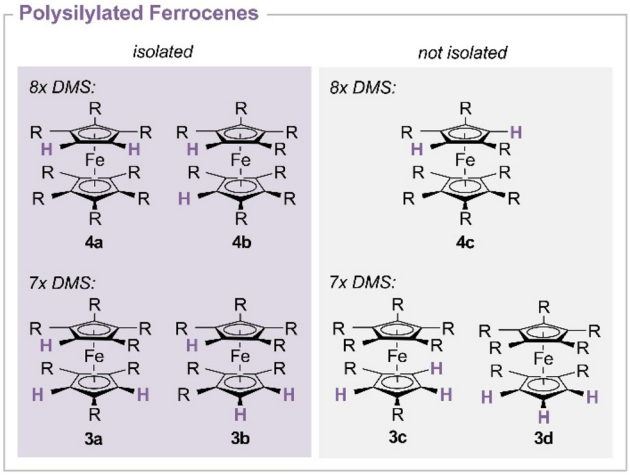

Fig. 1 Possible regioisomers of $[FeC_{10}DMS_8H_2]$ and $[FeC_{10}DMS_7H_3]$.

decakis(dimethylsilyl)ferrocene separated, but also their corresponding regioisomers in milligram scale. Considering the heptakis- and octakis(dimethylsilyl)ferrocene, in principle four or three possible regioisomers, respectively, exist. However, only four of the seven possible compounds were isolated. The distribution of the observed substitutional pattern reveals that silylation occurs equally at both Cp ligands rather than a consecutive silylation of only one Cp ligand, as metallocenes **3c**, **3d** and **4c** with a tetrakis(dimethylsilyl)cyclopentadienyl ligand were dominantly formed (Fig. 1, purple). This indicates that silylation might have been hampered due to strong steric hindrance.

Single crystals of all isolated compounds were obtained by recrystallization from $MeOH/H_2O$ or THF mixtures and analyzed *via* single-crystal XRD. The steric influence of the polysilylated cyclopentadienyl ligands becomes clear from several features: for the sterically overcrowded metallocenes a staggered conformation is preferred. In the solid state structures extraordinarily large Fe–C bond lengths up to 2.118(1) Å in comparison with that of unsubstituted ferrocene (Fe–C: 2.051(2)–2.063(2) Å (ref. 39)) are observed, indicating repulsion of the parallel cyclopentadienyl ligands. Furthermore, a bent structure for the cyclopentadienyl ligands is observed, as almost all Si atoms are found out of the Cp plane (Table 1, $Si–Cp^{plane}$). This effect is the most pronounced in the $[FeC_{10}DMS_{10}]$ (**6**) and $[FeC_{10}DMS_9H]$ (**5**) structures which exhibit even larger angulations in 1,1′,2,2′,4,4′-hexakis(trimethylsilyl)ferrocene (12.8° (ref. 40)). Moreover, the DMS groups on the persilylated ligand prefer to order in a highly symmetric circular manner. As a result, two sets of methyl groups are found pointing towards or away from the iron center while the silicon–hydrogen bond is in the same plane as the Cp ligand. In unsymmetrically silylated ferrocenes (*e.g.* **3a**, **4a**), the repulsive interaction is compensated by tilting of the respective ferrocene (Table 1, $Cp–Cp'^{tilt}$), whereupon the parallel orientation of the DMS substituents on the less substituted Cp ligands is repealed (Fig. 2).

Table 1 Selected structural parameters

Compound	Distances/Å Fe–C	Angles/° $Cp–Cp'^{tilt}$	$Si–Cp^{plane}$
$FeC_{10}DMS_{10}$ (**6**)	2.000(8)–2.118(2)	0.0(1)	15.1(2)–13.2(1)
$FeC_{10}DMS_9H$ (**5**)[a]	2.044(17)–2.115(3)	3.0(4), 3.5(1)	31.7(3)–9.5(3)
$FeC_{10}DMS_8H_2$ (**4a**)	2.055(5)–2.111(6)	8.0(2)	20.4(2)–5.4(2)
$FeC_{10}DMS_8H_2$ (**4b**)[a]	2.051(3)–2.115(3)	2.5(1), 3.8(1)	10.1(1)–3.6(1)
$FeC_{10}DMS_7H_3$ (**3a**)	2.056(2)–2.097(2)	5.0(1)	10.4(1)–1.3(1)
$FeC_{10}DMS_7H_3$ (**3b**)	2.057(2)–2.099(2)	3.1(1)	11.4(1)–3.3(1)

[a] Multiple metallocene molecules are found within the asymmetric unit.

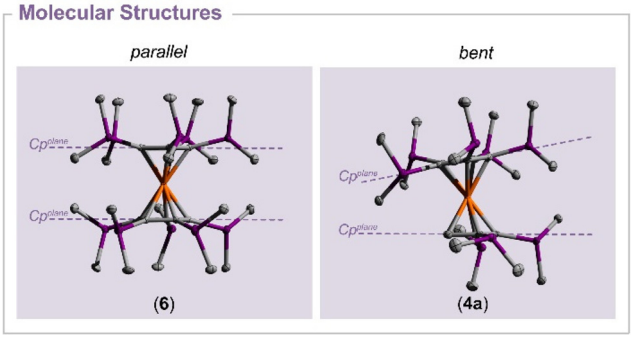

Fig. 2 Molecular structures in solid state of compounds $[FeC_{10}DMS_8H_2]$ (**4a**) and $[FeC_{10}DMS_{10}]$ (**6**). Ellipsoids are drawn with a 50% probability level. Hydrogen atoms and disorder were omitted for clarity. Dashed lines display the plane of the five-membered Cp ring. Color code: purple – silicon, orange – iron, grey – carbon.

The repulsive interactions cause signs of rotational hindrance regarding the DMS groups in the ^1H and $^{13}C\{^1H\}$ NMR spectra. Considering rotatable silyl groups, the compound $[FeC_{10}DMS_{10}]$ (**6**) should show one signal for the magnetically equivalent DMS methyl protons in the ^1H and $^{13}C\{^1H\}$ NMR spectra, respectively. However, two signals at δ = 0.76 and 0.09 ppm with an integral ratio of 1 : 1 in the ^1H spectrum and at δ = 2.41 and −0.18 ppm in the $^{13}C\{^1H\}$ spectrum are observed instead, as the pairs of methyl groups do not resolve together and are consequently chemically inequivalent. A similar behavior is observed for compounds **5** and **4b** with $[C_5(DMS)_4H]^-$ ligands. The metallocenes with threefold silylated cyclopentadienyl ligands exhibit lower rotational barriers for the silyl groups next to the unsubstituted position. Hence, heptasilyl isomers **3a** and **3b** do not show the expected four methyl signals in their $^{13}C\{^1H\}$ NMR spectra, but instead six signals, while the octasilyl compound **4a** exhibits four differentiated $^{13}C\{^1H\}$ signals instead of three expected in the absence of rotational hindrance.

Substitution of the cyclopentadienyl protons typically results in significant electronic and electrochemical changes in metallocenes as HOMO and LUMO energies are shifted. In classical acceptor-substituted compounds, *e.g.* haloferrocenes, the substituents mainly stabilize the HOMO while weakly de-

stabilizing the LUMO,[41] resulting in high redox potentials for the reversible redox couple $Fe^{+II/+III}$.[42] In silylated ferrocenes, *e.g.* $[Fe(C_5(TMS)H_4)_2]$ (0.01 V *vs.* FcH), similar redox potentials to those of unsubstituted ferrocene are observed.[43] The electrochemical properties of the polysilylated metallocenes **3** to **6** were determined by cyclic voltammetry in THF and referenced against the FcH/FcH^+ redox couple. All compounds exhibit a reversible one-electron oxidation with half-wave potentials between $E_{1/2}$ = 0.161 V and 0.172 V, indicating that the silyl groups do not affect the HOMO energies significantly.

In contrast to this, the UV/VIS spectra of isolated silylferrocenes **3** to **6** indicate decreasing HOMO–LUMO energy gaps. Those spectra were recorded in *n*-hexane (Fig. 3). Unsubstituted ferrocene exhibits an absorption band at λ = 441 nm in the visible regime corresponding to the unresolved $^1A_1 \rightarrow {}^1E_1$ and $^1A_1 \rightarrow {}^1E_2$ spin-allowed d–d transitions, explaining the orange color of this compound.[41,44] Incorporation of dimethylsilyl groups causes a bathochromic shift yielding a color transition from red to purple from heptakis- to decakis (dimethylsilyl)ferrocene. This shift has been observed in previously reported polysilylated ferrocenes[2,45,46] as well. However, in the spectra of silylferrocenes **3** to **6** this band is accompanied by a shoulder which is most pronounced in the spectrum of $[FeC_{10}DMS_{10}]$ (**6**).

To explain these findings, density functional theory (DFT) calculations were performed, comparing unsubstituted ferrocene, $[FeCp_2]$, with the persilylated derivative (**6**) (ωB97X-D/def2-TZVPP(D)//r^2SCAN-3c level, see the ESI† for details). For $[FeCp_2]$, the expected D_{5h} symmetric minimum is found, with the usual D_{5d} transition state for the rotation of the Cp ligands (at a free energy of about 5 kJ mol^{-1}, consistent with the well-known free rotation in solution[47]). Time-dependent DFT calculations of the lowest excitation energies give a band at λ = 461 nm, for a $^1A_1 \rightarrow {}^1E_1$ transition (in D_5 notation) and two additional bands at λ = 351 nm and 512 nm, arising from the second $^1A_1 \rightarrow {}^1E_1$ and the formally forbidden $^1A_1 \rightarrow {}^1E_2$ transitions, respectively (ESI, Fig. S78†). The overall spectrum agrees very well with the experimentally determined spectrum.

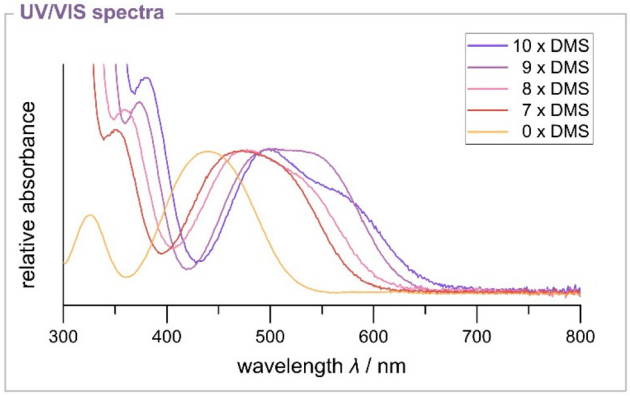

Fig. 3 Normalized UV/VIS spectra of compounds $[FeC_{10}DMS_{10}]$ (**6**), $[FeC_{10}DMS_9H]$ (**5**), $[FeC_{10}DMS_8H_2]$ (**4b**), $[FeC_{10}DMS_7H_3]$ (**3b**) and ferrocene in *n*-hexane.

It is likely that the closeness of the two lowest excitation energies and the similar intensities (when also considering contributions from the D_{5d} transition state) lead to a broadening of the peak, without a clearly discernible shoulder.

Replacing the Cp–hydrogen atoms with DMS groups so that the fivefold axis of the Cp ligand is retained results in two possible conformers (of D_5 and S_{10} symmetry, respectively) which differ in the relative orientation of the Si–H bonds on the two rings. The electronic energy difference between the two conformers vanishes, consistent with the experimentally observed disorder in the crystal structure of **6** (ESI, Fig. S79†). Based on our calculations, these two conformers lead to qualitatively different spectra (ESI, Fig. S78†). A low-energy shoulder is found for the S_{10} structure but not for the D_5 structure. However, the D_5 conformer exhibits much larger intensities, as the $^1A_1 \rightarrow {}^1E_1$ transition becomes dipole-allowed. We suspect that the shoulder observed experimentally (Fig. 3) may be due to a significant contribution to these low-energy regions of the spectrum from further areas on the conformational energy surface that are accessed dynamically at experimental temperatures. Contributions from different, energetically similar structures may be expected also for the hepta-, octa- and nonasilylated compounds, explaining their comparable band shapes.

Most notably, the TDDFT calculations clearly confirm the overall bathochromic shift of the spectrum upon silylation. NPA charges (ESI, Table S78†) become more positive from $[FeCp_2]$ to **6**. Most of this substituent effect seems to be structural, caused by the substantially longer Fe–C distances in **6**. Computations on $[FeCp_2]$ with the carbon positions of **6** do already provide most of the changes in charges and band positions, while finally adding the DMS substituents has a relatively small effect.

Closer analysis of the MOs and of the character of the electronic excitations shows that the degenerate HOMO in **6** is genuinely nonbonding (with d_{xy} and $d_{x^2-y^2}$ character) and thus also changes very little (by less than 0.15 eV) upon expanding the Fe–C distances and upon finally adding the DMS substituents. This is consistent with the small effect of the silyl substituents on the redox potentials (see above). The low-lying excitations are out of this HOMO and out of another high-lying occupied MO with predominant metal d_{z^2} character. This MO, which is very slightly σ-antibonding, drops in energy by about 0.25 eV upon bond expansion but goes up by 0.17 eV when adding the DMS substituents, thus staying also almost unchanged overall compared to $[FeCp_2]$. The changes in the band gap and low-lying excitation energies from $[FeCp_2]$ to **6** are thus largely due to changes in the virtual MO energies. In particular, the (twofold degenerate) LUMO comes down by 0.47 eV upon bond lengthening and by another 0.20 eV upon adding the DMS substituents. The LUMO is clearly π-antibonding and becomes less antibonding for the silyl-substituted ferrocenes, thus explaining the bathochromic shifts.

1,1-Substituted ferrocenes

Although we were able to isolate the persilylated derivative $[FeC_{10}DMS_{10}]$ (**6**) the demonstrated synthetic approach is

inconvenient for further synthetic applications in terms of selectivity and experimental effort. In order to generate highly overcrowded metallocenes in a selective manner we modified the substitutional pattern to 1,1′-disubstituted ferrocenes. Here the presence of methyl groups should in part compensate the electron-withdrawing and steric effects of the silyl substituents. The polybrominated compound $[FeC_{10}Br_8Me_2]$ (**7**) was synthesized by eightfold mercuration of 1,1′-dimethylferrocene followed by bromination with KBr_3, analogous to the synthetic protocol for decabromoferrocene.[34] The silylation of the corresponding metallocene was carried out with elemental magnesium and DMSCl in anhydrous THF. In contrast to the analogous reaction of decabromoferrocene the perfunctionalized derivative was obtained selectively in high yields (88%). Due to the high selectivity of the reaction step the purification of the substrates is accomplished easily by recrystallization instead of complex chromatographic methods. The obtained compound $[FeC_{10}DMS_8Me_2]$ (**8**) was analyzed by NMR, UV/VIS and single-crystal XRD. The polysilylated metallocenes show similar features as $[FeC_{10}DMS_{10}]$ (**6**). In the ^1H and $^{13}C\{^1H\}$ NMR spectra the signals which were assigned to the methyl groups attached to silicon split into a set of four signals indicating again a hindered rotation along the $Si–C^{Cp}$ axis. In the UV/VIS spectra the observed absorption maximum in the visible region at λ_{max} = 490 nm is again red-shifted, indicating decreased HOMO–LUMO energy gaps. The observed wavelengths are similar to those of $[FeC_{10}DMS_8H_2]$ (**4b**: λ_{max} = 495 nm) with tetrasilylated Cp ligands. Single crystals of compound **8** were obtained upon crystallization from MeOH/THF mixtures. The molecular structure shows again elongated metal–Cp bonds of 2.082(4)–2.099(4) Å compared to those of unsubstituted ferrocene (Fe–C: 2.051(2)–2.063(2) Å 39). The Cp rings deviate from a parallel arrangement by only 4.6(2)° due to the lower steric demand of the methyl groups. The silyl groups are found out of the Cp plane (5.3–20.9°) in spite of the reduced steric demand induced by the methyl groups.

Conclusions

The focus of this work was to find appropriate methods for the generation of highly silylated ferrocenes to investigate the effects of steric overload and charge stabilization by the silyl groups.[48] Reactions were carried out by metalation of bromoferrocenes $[FeC_{10}Br_{10}]$ and $[FeC_{10}Br_8Me_2]$ followed by quenching with DMSCl. We observed that the introduction of silyl groups inhibits further silylation yielding only a mixture of polysilylated compounds $[FeC_{10}DMS_nH_{10-n}]$ (n = 10, 9, 8) containing the targeted decasilylated ferrocene in low yields. The reactivity of the polymetalated intermediates and the selectivity of the products drastically improved when electron donating groups were applied and the corresponding octasilylated metallocenes $[FeC_{10}DMS_8Me_2]$ were isolated purely in good yields despite the sterically demanding substituents.

Mixtures of polysilylated metallocenes $[FeC_{10}DMS_nH_{10-n}]$ (n = 10, 9, 8, 7) were successfully separated by HPLC allowing a systematic study on silylation effects on ferrocene by XRD, CV, NMR and UV/VIS spectroscopy. Here, the steric overcrowding is reflected by significant rotational hindrance of the tetra- and pentasilylated cyclopentadienyl ligands regarding the DMS groups and greater ordering. Furthermore, the cyclopentadienyl ligands are found to exhibit distortions from planarity within the molecular structure.[49] The maximum UV/VIS absorbances are systematically red-shifted with further silylation indicating decreased energy gaps between occupied and virtual MOs. DFT calculations show that this is largely due to the lengthening of the Fe–C bonds caused by the steric crowding induced by the silyl substituents. The occupied frontier MOs are largely nonbonding in nature and thus not affected much by the substitution, in agreement with small changes in the redox potentials. But the metal–ligand antibonding character of the lowest-lying virtual MOs is reduced compared to that of the parent ferrocene, giving rise to the observed red shifts.

The approach of exploiting sterically demanding and electron donating groups to force high degrees of silylation allows the isolation of sterically overcrowded cyclopentadienyl compounds on multigram scale. Even a subsequent methylation to obtain the trimethylsilyl substituted analogues should be feasible to obtain chemically more inert and increasingly overloaded compounds. In the future, the syntheses of other main group, transition metal or lanthanide or actinide complexes with persilylated cyclopentadienyl ligands could be of great interest.

Author contributions

S. M. R. designed the project and wrote the manuscript. Furthermore, she performed the synthesis, recorded cyclic voltammetry and UV/VIS data as well as prepared, measured and solved the single-crystal XRD data. R. S. and P. S. R. performed experiments and analyzed the data. Both authors were supervised by S. M. R. M. R. and M. K. performed the quantum chemical calculations and revised the manuscript. C. F. designed the HPLC experiments. M. M. supervised the project and revised the manuscript.

Conflicts of interest

There are no conflicts to declare.

Acknowledgements

This study was funded by Deutsche Forschungsgemeinschaft (DFG) – project number: 387284271 – SFB 1349. We would like to acknowledge the assistance of the Core Facility BioSupraMol supported by the DFG.

References

1 J. Okuda, *Chem. Ber.*, 1989, **122**, 1075–1077.
2 J. Okuda and E. Herdtweck, *J. Organomet. Chem.*, 1989, **373**, 99–105.
3 M. P. Plesniak, X. Just-Baringo, F. Ortu, D. P. Mills and D. J. Procter, *Chem. Commun.*, 2016, **52**, 13503–13506.
4 D. Cui, O. Tardif and Z. Hou, *J. Am. Chem. Soc.*, 2004, **126**, 1312–1313.
5 F. Ortu, J. Lui, M. Burton, M. Fowler, A. Formanuik, M.-E. Boulon, N. F. Chilton and D. P. Mills, *Inorg. Chem.*, 2017, **56**, 2496–2505.
6 D. Cui, M. Nishiura and Z. Hou, *Angew. Chem., Int. Ed.*, 2005, **44**, 959–962.
7 W.-X. Zhang, Z. Wang, M. Nishiura, Z. Xi and Z. Hou, *J. Am. Chem. Soc.*, 2011, **133**, 5712–5715.
8 L. M. Engelhardt, P. C. Junk, C. L. Raston and A. H. White, *J. Chem. Soc., Chem. Commun.*, 1988, 1500–1501.
9 A. H. Cowley, P. Jutzi, F. X. Kohl, J. G. Lasch, N. C. Norman and E. Schlüter, *Angew. Chem.*, 1984, **96**, 603–604.
10 M. J. Harvey, T. P. Hanusa and M. Pink, *J. Chem. Soc., Dalton Trans.*, 2001, 1128–1130.
11 P. Jutzi, E. Schlüter, M. B. Hursthouse, A. M. Arif and R. L. Short, *J. Organomet. Chem.*, 1986, **299**, 285–295.
12 M. Westerhausen, S. Schneiderbauer, N. Makropoulos, M. Warchhold, H. Nöth, H. Piotrowski and K. Karaghiosoff, *Organometallics*, 2002, **21**, 4335–4341.
13 C. H. Winter, X. X. Zhou and M. J. Heeg, *Inorg. Chem.*, 1992, **31**, 1808–1815.
14 A. Sekiguchi, T. Nakanishi, C. Kabuto and H. Sakurai, *J. Am. Chem. Soc.*, 1989, **111**, 3748–3750.
15 A. Sekiguchi, M. Ichinohe, C. Kabuto and H. Sakurai, *Organometallics*, 1995, **14**, 1092–1094.
16 A. Sekiguchi, T. Matsuo, K. Ebata and H. Sakurai, *Chem. Lett.*, 1996, **25**, 1133–1134.
17 A. Sekiguchi, T. Matsuo and H. Watanabe, *J. Am. Chem. Soc.*, 2000, **122**, 5652–5653.
18 A. Sekiguchi, K. Ebata, C. Kabuto and H. Sakurai, *J. Am. Chem. Soc.*, 1991, **113**, 1465–1466.
19 J. C. Wedal, J. M. Barlow, J. W. Ziller, J. Y. Yang and W. J. Evans, *Chem. Sci.*, 2021, **12**, 8501–8511.
20 M. R. Trinh, J. C. Wedal and W. J. Evans, *Dalton Trans.*, 2021, **50**, 14384–14389.
21 R. R. Langeslay, M. E. Fieser, J. W. Ziller, F. Furche and W. J. Evans, *Chem. Sci.*, 2015, **6**, 517–521.
22 R. R. Langeslay, M. E. Fieser, J. W. Ziller, F. Furche and W. J. Evans, *J. Am. Chem. Soc.*, 2016, **138**, 4036–4045.
23 M. R. MacDonald, J. E. Bates, J. W. Ziller, F. Furche and W. J. Evans, *J. Am. Chem. Soc.*, 2013, **135**, 9857–9868.
24 M. E. Fieser, M. R. MacDonald, B. T. Krull, J. E. Bates, J. W. Ziller, F. Furche and W. J. Evans, *J. Am. Chem. Soc.*, 2015, **137**, 369–382.
25 K. Sünkel and J. Hofmann, *Organometallics*, 1992, **11**, 3923–3925.
26 A. Sekiguchi, Y. Sugai, K. Ebata, C. Kabuto and H. Sakurai, *J. Am. Chem. Soc.*, 1993, **115**, 1144–1146.
27 M. S. Miftakhov, G. A. Tolstikov and S. I. Lomakina, *Zh. Obshch. Khim.*, 1976, **46**, 2754–2754.
28 P. Jutzi, E. Schlüter, C. Krüger and S. Pohl, *Angew. Chem., Int. Ed. Engl.*, 1983, **22**, 944–944.
29 M. A. Edelman, P. B. Hitchcock, M. F. Lappert, D.-S. Liu and S. Tian, *J. Organomet. Chem.*, 1998, **550**, 397–808.
30 H. Chen, P. Jutzi, W. Leffers, M. M. Olmstead and P. P. Power, *Organometallics*, 1991, **10**, 1282–1286.
31 C. P. Morley and P. Jutzi, *Organometallics*, 1987, **6**, 1084–1090.
32 J. Okuda and E. Herdtweck, *Chem. Ber.*, 1988, **121**, 1899–1905.
33 I. R. Butler, D. M. Evans, P. N. Horton, S. J. Coles and P. J. Murphy, *Organometallics*, 2021, **40**, 600–605.
34 S. M. Rupf, I. S. Dimitrova, G. Schröder and M. Malischewski, *Organometallics*, 2022, **41**, 1261–1267.
35 S. M. Rupf, G. Schröder, R. Sievers and M. Malischewski, *Chem. – Eur. J.*, 2021, **27**, 5125–5129.
36 P. Štěpnička, *Dalton Trans.*, 2022, **51**, 8085–8102.
37 C. H. Winter and K. N. Seneviratne, *Comments Inorg. Chem.*, 1996, **19**, 1–23.
38 J. R. Baran Jr., C. Hendrickson, D. A. Laude Jr. and R. J. Lagow, *J. Org. Chem.*, 1992, **57**, 3759–3760.
39 P. Seiler and J. D. Dunitz, *Acta Crystallogr., Sect. B: Struct. Crystallogr. Cryst. Chem.*, 1982, **38**, 1741–1745.
40 J. Okuda, *J. Organomet. Chem.*, 1989, **376**, C1–C4.
41 M. S. Inkpen, S. Du, M. Hildebrand, A. J. P. White, N. M. Harrison, T. Albrecht and N. J. Long, *Organometallics*, 2015, **34**, 5461–5469.
42 D. A. Khobragade, S. G. Mahamulkar, L. Pospíšil, I. Císarová, L. Rulísek and U. Jahn, *Chem. – Eur. J.*, 2012, **18**, 12267–12277.
43 A. Abri and A. abbaszad Rafe, *J. Chin. Chem. Soc.*, 2015, **62**, 273–279.
44 Y. S. Sohn, D. N. Hendrickson and H. B. Gray, *J. Am. Chem. Soc.*, 1971, **93**, 3603–3612.
45 O. J. Curnow, G. M. Fern, S. Klaib, U. Böhme, H. Lang and R. Holze, *J. Electroanal. Chem.*, 2005, **585**, 167–171.
46 J. Okuda, R. W. Albach and E. Herdtweck, *Polyhedron*, 1991, **10**, 1741–1748.
47 M. Rosenblum and R. B. Woodward, *J. Am. Chem. Soc.*, 1958, **80**, 5443–5449.
48 A previous version of the manuscript has been deposited on a preprint server: S. M. Rupf, R. Sievers, P. S. Riemann, M. Reimann, K. Kaupp, C. Fasting and M. Malischewski, *ChemRxiv*, 2023, DOI: **10.26434/chemrxiv-2023-538rg**.
49 Deposition numbers CCDC 2248053–2248061 contain the supplementary crystallographic data for this paper.†